Available online at www.sciencedirect.com
SCIENCE DIRECT®
Agricultural and Forest Meteorology 136 (2006) 159–174
AGRICULTURAL AND FOREST METEOROLOGY
www.elsevier.com/locate/agrformet

Atmospheric reactive nitrogen concentration and flux budgets at a Northeastern U.S. forest site☆

Cassandra Volpe Horii [a,*], J. William Munger [a], Steven C. Wofsy [a], Mark Zahniser [b], David Nelson [b], J. Barry McManus [b]

[a] *Division of Engineering and Applied Sciences and Department of Earth and Planetary Science, Harvard University, 20 Oxford Street, Cambridge, MA 02138, USA*
[b] *Aerodyne Research, Inc., 45 Manning Road, Billerica, MA 01821, USA*

Abstract

We report concentrations of atmospheric NO_x, nitric acid (HNO_3), peroxyacetyl nitrate (PAN), and NO_y; eddy covariance fluxes of NO_x and NO_y; inferred fluxes of HNO_3 at the mixed deciduous Harvard Forest field site, June–November 2000. A novel Tunable Diode Laser Absorption Spectrometer (TDLAS) produced sensitive, hourly HNO_3 concentration data, which were used to evaluate systematic error in the Dry Deposition Inferential Method (DDIM), often employed to estimate weekly HNO_3 flux at deposition monitoring network sites. Due to the weak diurnal variation in HNO_3 concentration at Harvard Forest, no systematic bias was found in the application of this method to compute daily and weekly average fluxes. The sum of individually measured reactive nitrogen species concentrations and fluxes were approximately equal to total NO_y concentrations and fluxes for clean Northwesterly flows, but fell short of the total NO_y values for the more polluted Southwesterly transport regime. The concentration and deposition velocity of the unmeasured reactive nitrogen compounds were consistent with prior estimates and recent measurements of alkyl- and hydroxyalkyl nitrates, suggesting that these compounds play an important role in reactive nitrogen deposition processes where anthropogenic NO_x emissions and natural hydrocarbons are present.

Keywords: Deciduous forest; Reactive nitrogen (NO_y); Nitric acid (HNO_3); Nitrogen deposition

1. Introduction

The partitioning of total reactive nitrogen, $NO_y = NO + NO_2 + NO_3 + 2N_2O_5 + HNO_3$ + peroxyacetyl nitrate (PAN) + other organic nitrates + aerosol nitrate, among the individual species has direct effects on photochemical production of ozone in rural and urban areas, on deposition of acidic species to ecosystems, on ecosystem nutrient status, and on the export of atmospheric nitrogen from the continent to the global troposphere. Reactive nitrogen enters the atmosphere primarily as NO emitted by combustion or soil microbes, with additional contributions from lightning, ammonia oxidation, emission from the oceans, and transport from the stratosphere. NO and NO_2 (the NO_x radicals) interconvert rapidly in the troposphere, with reaction timescales on the order of minutes. Conversion of NO_x to nitric acid (HNO_3) and subsequent wet and dry deposition occur on longer timescales, hours to days. Such deposition is widely held to be the primary tropospheric loss process for reactive nitrogen. Atmospheric NO_x is converted to HNO_3 via both homogeneous and heterogeneous

DOI of original article: 10.1016/j.agrformet.2004.08.009.
☆ This paper was previously published in error in Agricultural and Forest Meteorology, vol. 133(1–4). The publisher apologizes for this error.
* Corresponding author. Tel.: +1 617 495 5361; fax: +1 617 495 2768.
E-mail address: cvhorii@post.harvard.edu (C.V. Horii).

0168-1923/$ – see front matter © 2005 Elsevier B.V. All rights reserved.
doi:10.1016/j.agrformet.2006.03.005

chemical pathways. Because recycling of HNO_3 back to NO_x is inefficient in the troposphere compared to wet and dry deposition, oxidation of NO_x to HNO_3 terminates the NO_x photochemistry that produces O_3. NO_x also forms temporary non-radical reservoir species such as PAN and other organic nitrates, allowing alternative deposition pathways or export to remote regions where radicals can be regenerated.

The nitrate provided to ecosystems by reactive nitrogen deposition acts as an essential nutrient that may stimulate forests and crops if the dose is not too high. However, at high deposition rates excess nitrate is harmful; loss of base cations, mobilization of toxic elements such as aluminum in soils, disruption of nutrient balances, and other impacts have been observed (Aber et al., 1998; Magill et al., 2000). Due to the complexity of nutrient cycling in ecosystems, long-term effects on ecosystem growth due to deposition of acidic species such as HNO_3 may take many decades to become apparent, and have important links to global climate through impacts on carbon uptake (Tomlinson, 2003). Deposition of HNO_3 is the second most important atmospheric source of acidity after sulfuric acid in the Northeastern U.S. (U.S. Environmental Protection Agency, 2001). The abundance of sulfuric acid and sulfur deposition in general have declined since 1990 due to regulation of sulfur dioxide emissions, largely from coal-burning power plants. Nitrogen deposition (total wet and dry), however, has remained approximately constant over the same period (Baumgardner et al., 2002). If these trends continue, HNO_3 may become an even more important contributor to acid deposition. Weekly HNO_3 dry deposition estimates from the Clean Air Status and Trends Network (CASTNet) suggest that dry and wet HNO_3 deposition contribute nearly equally to the total (U.S. EPA, 2001).

Because the distribution of total atmospheric reactive nitrogen among individual species has implications for both atmospheric chemistry and ecosystem conditions, it is important to measure the concentrations and fluxes of the individual species. Comparisons between the sum of atmospheric concentrations of individual NO_y species, $\sum[NO_y]_i$, and total $[NO_y]$, measured by catalytic conversion (on hot gold or molybdenum) to NO, have been conducted at continental rural sites (e.g. Parrish et al., 1993; Aneja et al., 1996; Thornberry et al., 2001; Hayden et al., 2003), at coastal sites (e.g. Harrison et al., 1999), and in the remote free troposphere (e.g. Bradshaw et al., 2000). Differences sometimes observed between $[NO_y]$ and $\sum[NO_y]_i$ could be due in part to interference of reduced nitrogen species (e.g. NH_3, HCN, and other organic molecules with direct C–N bonds) with the NO_y measurements (Kliner et al., 1997; Bradshaw et al., 1998; Harrison et al., 1999), but unmeasured species, such as alkyl and hydroxyalkyl nitrates, have also been implicated (Day et al., 2003; Rosen et al., 2004).

Few studies have attempted to speciate the reactive nitrogen deposition budget, and consequently, considerable uncertainty attaches to the importance of processes controlling the fluxes of individual species. Munger et al. (1996, 1998) observed concentrations and eddy covariance fluxes of NO_y and NO_x, showing that NO_x was not a major contributor to deposition, and implying that nearly all dry deposition of NO_y occurs in the form of rapidly depositing species such as HNO_3. They indirectly inferred a summertime contribution due to organic hydroxyalkyl nitrates formed during the oxidation of biogenic hydrocarbons (isoprene and monoterpenes). Recently, we confirmed through eddy covariance flux measurements that net deposition of NO_x is small compared to NO_y fluxes (Horii et al., 2004). Recent measurements suggest that PAN deposition to vegetation is controlled by leaf stomatal aperture, varying with species and leaf internal PAN concentration (Sparks et al., 2003). Though Sparks et al. suggest that PAN deposition may play a more important role in the nitrogen flux budget than indicated by previous estimates (Shepson et al., 1992; Schrimpf et al., 1996; McFadyen and Neil Cape, 1999), the measured PAN deposition rates were slower and more variable than those of HNO_3.

Due in part to its tendency to adsorb onto surfaces, HNO_3 measurement techniques with demonstrated accuracy, high precision, and a lack of interference have taken decades to develop. Increasingly reliable methods have appeared over the last several years. Filter packs and denuders of various designs are employed for routine monitoring (e.g. Harrison et al., 1999; Rosman et al., 2001; Clarke et al., 1997). These techniques often require collection times on the order of hours to days, after which the filter or denuder is removed, extracted, and processed to detect NO_3^- in solution by ion chromatography. Mist chamber techniques rely on capture and dissolution of HNO_3 and detection by ion chromatography; recent implementations have the advantage of much shorter integration times (minutes) and thorough calibration procedures, which have greatly reduced the uncertainties associated with the measurements (cf. Talbot et al., 1997; Bradshaw et al., 1998). Day et al. (2003) employ thermal dissociation of NO_y compounds at calibrated temperatures followed by laser-induced fluorescence detection of NO_2 to measure HNO_3, peroxy nitrates, and alkyl nitrates.

Chemical Ionization Mass Spectrometers (CIMS) also achieve high sensitivity (<50 pmol mol^{-1}), lack of interferences, and short integration times for HNO_3 concentration measurements (Huey et al., 1998; Mauldin et al., 1998; Fehsenfeld et al., 1998; Miller et al., 2000; Furutani and Akimoto, 2002). The heated, constant-flow permeation devices used for most CIMS calibration procedures require long stabilization times and extremely constant temperatures and flow rates, and have found effective applications in short field deployments and aircraft applications.

Tunable Diode Laser Absorption Spectroscopy (TDLAS) provides a useful alternative for continuous, unattended field monitoring of HNO_3. The TDLAS instrument used to measure HNO_3 in this study employs recent advances in long path length/low volume absorption cells, inlet material and design, and real-time data processing to achieve a spectroscopically calibrated measurement of HNO_3 concentration. A prototype HNO_3 TDLAS instrument participated in an informal intercomparison with the CIMS HNO_3 instrument described by Huey et al. (1998) in 1996. The TDLAS compared well with the CIMS results over a wide range of concentrations, ambient relative humidity, and pollution levels (Horii et al., 1999).

We added the TDLAS to the long-term, existing suite of NO_y, NO_x, and auxiliary measurements at the Harvard Forest Environmental Measurement Site (HFEMS) in 2000 in order to produce the reactive nitrogen concentration and flux budgets reported here for June–November. Direct measurements of concentrations (NO_y, NO, NO_2, HNO_3, and PAN) and eddy covariance fluxes (NO_y and NO_x) are included. The flux of HNO_3 was estimated using a standard Dry Deposition Inferential Method (DDIM), versions of which are employed widely by U.S. deposition monitoring networks. The time resolution of the HFEMS HNO_3 dataset also enabled testing of the DDIM for possible biases that may be introduced when it is used with daily or weekly HNO_3 concentration measurements in routine monitoring networks. The NO_y budgets presented here enabled determination of the concentration and average deposition velocity of a class of rapidly depositing, non-HNO_3 compounds present only when the site received polluted air from the Southwest.

2. Methods

2.1. Site description

The Harvard Forest Environmental Measurement Site is in a 50–70-year-old mixed deciduous forest of red oak and red maple, with scattered hemlock, red and white pine in central Massachusetts (42.54N, 72.18W; elevation, 340 m). The moderately hilly landscape is approximately 95% forested, with the nearest paved road more than 1.5 km distant and the nearest small town more than 10 km away. Extensive study of the local meteorology at the site has indicated that it is suitable for eddy covariance flux measurements due to a lack of anomalous flow patterns and an energy budget that is closed to within 15% (Moore et al., 1996; Goulden et al., 1996). The leaf area index (LAI) during summer is approximately 3.4 (determined by leaf collection), stem and twig area index (STAI) is 0.9, and the canopy height near the towers is approximately 20 m, with a few individuals as tall as 23 m. Northwesterly and Southwesterly winds dominate; the former bringing relatively cool, dry, unpolluted air, and the latter bringing warm, humid, significantly more polluted air to the site (Moody et al., 1998; Munger et al., 1996). Emissions from the Boston area, 100 km to the East, rarely reach the site due to the prevailing Westerly winds. In terms of vegetation, terrain, transport, and anthropogenic sources of emissions, the HFEMS is similar to much of the semi-rural inland Northeastern U.S.

We utilized two towers for this study. The first was a permanent 30 m Rohn 25G tower, used since 1990 to measure eddy covariance fluxes of CO_2, NO_y, and O_3, along with vertical profiles of NO, NO_2, O_3, and other species. The second was a temporary 23 m steel scaffolding tower, situated about 100 m to the Southeast of the Rohn tower and outfitted with a sonic anemometer and a Tunable Diode Laser Absorption Spectrometer (TDLAS) configured to measure concentrations of HNO_3. The TDLAS also measured concentrations and eddy covariance fluxes of NO_2 during the same period. Physical constraints limited the height of the second tower and prevented matching the measurement height of the TDLAS (22 m) with the measurement height of NO_y, NO_x, and PAN (29 m) on the first tower. In order to confirm that the different measurement heights on the two towers were in the same flux regime, we compared concurrently measured heat fluxes from the two sonic anemometers and found no significant differences (Fig. 1). Comparison of concurrent trace gas and other meteorological data has also shown that the two datasets are spatially coherent on the hourly timescale (Horii, 2002). Data from the two towers were matched and averaged into an hourly dataset, available at http://www-as.harvard.edu/chemistry/index.html.

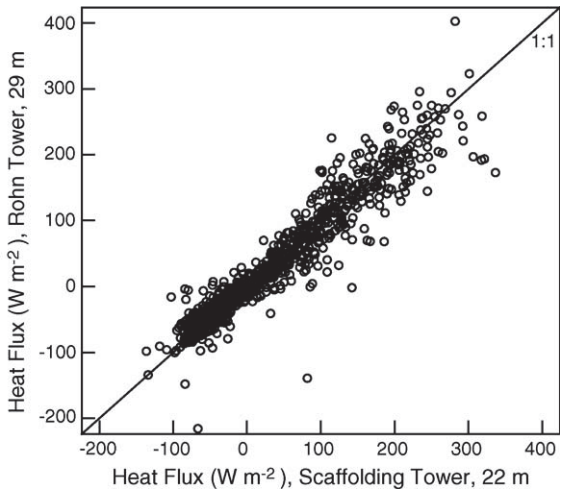

Fig. 1. Hourly heat fluxes measured by sonic anemometry at a height of 29 m on the Rohn tower (vertical axis) and at a height of 22 m on the scaffolding tower (horizontal axis), shown with a 1:1 line.

2.2. Instrumentation

2.2.1. HNO_3

The concentration of HNO_3 at the HFEMS was measured using a Tunable Diode Laser Absorption Spectrometer. The spectrometer itself was located on the tower's top platform, at a height of 19 m, with a 3 m inlet extending to a height of 22 m, and with supporting electronics and pumps located on lower tower platforms and in an enclosure at the base of the tower. The TDLAS specifically and quantitatively measured gas-phase HNO_3 by fitting in real-time several absorption lines near 1720 cm^{-1} to eliminate interferences from other substances such as PAN, hydroxyalkyl nitrates, NO_x, and fine aerosols (note that these species, and aerosols smaller than ~1 μm diameter, were included in the NO_y measurement). The instrument used a long path/low volume astigmatic Herriott absorption cell, developed at Aerodyne Research, Inc. (ARI), which provided a light path length of 210 m in a volume of 5 L (McManus et al., 1995). The cell was operated at low pressure, 2.5–4 kPa, with a flow rate of 10 L min^{-1} (STP). Under these conditions, the flushing time constant for the cell was approximately 0.5 s. The low-pressure cell drew its flow through a critical orifice at a right angle to the 100 L min^{-1} (STP), ambient pressure flow through the vertical 3 m inlet extension. In order to discriminate against non-HNO_3 spectral features, the sample cell flow was modulated with scrubbed ambient air, automatically injected at the tip of the low-pressure orifice every 10 min (a nylon filter effectively scrubbed the ambient air of HNO_3). Fine temperature control of the entire instrument also helped to match non-trace-gas spectral characteristics such as interference fringes between signal and background spectra.

The calibration of the TDLAS required laboratory determination of spectroscopic parameters (light path length, laser mode purity and frequency, laser tuning rate function, and laser line width), which were also checked in the field monthly using standard additions of HNO_3 from a permeation device, ambient water vapor, and a Germanium etalon. Independent cross-checks were obtained by comparing concentrations of H_2O measured using spectral lines in the HNO_3 spectral range with H_2O data from hygrometers on the main tower. One-second, integrated measurements of both zero air and a constant HNO_3 permeation tube source showed that the rms noise over a wide range of HNO_3 concentrations was 150–200 pmol mol^{-1}. HNO_3 precision was limited by the background noise of the photovoltaic detectors, the output power of the laser diode, and the finite reflectivity of the mirrors; it did not scale with concentration. Short- and long-term temperature and pressure instabilities within the instrument limited the improvement of precision obtained from longer integration times to a factor of 2–4.

An optimal material, fluorinated silane-coated fused silica quartz, was chosen for instrument and inlet surfaces in order to minimize wall effects for any strongly surface-reactive gas such as HNO_3 (for test results and discussion of different inlet materials, see Horii, 2002). The 3 m inlet was designed to keep the residence time short (characteristic flushing time = 1.5 s; turbulent half-power cutoff frequency = 2.9 Hz) and to exclude aerosols from the sample flow by inertial separation. HNO_3 was found to come into equilibrium with the walls of the inlet extension with a characteristic time constant of approximately 10 min. Although the TDLAS instrument alone would have been capable of high frequency (1 Hz, as employed for the NO_2 eddy covariance fluxes reported in Horii et al., 2004) measurements of ambient fluctuations in HNO_3 concentration, the inlet extension's longer equilibrium time removed much of the high frequency information for that species. However, laboratory tests with calibrated permeation devices showed that after allowing time for equilibration with the walls of the inlet extension, HNO_3 was transmitted to the measurement cell with near 100% efficiency. Because the inlet walls were not a permanent sink for HNO_3, the hourly average concentrations used in this analysis were not compromised. The hourly average concentration is also adequate for capturing the relevant chemical and depositional timescales associated with HNO_3 production and loss.

2.2.2. NO_y, NO_x, and PAN

NO_y measurements by reduction of total nitrogen oxide to NO on a hot gold catalyst in the presence of H_2 began in 1990 at the HFEMS and have continued with few interruptions since then. The catalyst was located at the inlet on the permanent tower, at a height of 29 m, to ensure accurate and rapid measurements of species such as HNO_3 that have a strong affinity for surfaces. Details of this method and instrument have been extensively documented and validated elsewhere (Munger et al., 1996).

Likewise, a NO_x Photolysis–Chemiluminescence (P–C) instrument has measured concentrations of NO_x radicals at heights of 29, 24.1, 18.3, 12.7, 7.5, 4.5, 0.8, and 0.3 m on the permanent tower since 1990, with methodological details and analysis presented in Munger et al. (1996). Calibrations of the P–C system were made using standard gas mixtures for NO and NO_2, traceable to NIST, four to five times per day. The NO_2 and NO standards were cross-calibrated by titrating the NO standard with O_3 and by analyzing both gas mixtures using the NO_y detector equipped with a hot gold catalyst for reducing NO_y to NO. From late August to mid-October 2000, this system was reconfigured to measure NO concentrations at 10 Hz at the 29 m sampling height, in order to determine eddy covariance fluxes for NO (Horii et al., 2004).

The TDLAS also measured NO_2 concentrations using a second diode laser and detector by the same method as HNO_3. The lack of inlet wall interactions for NO_2 made it possible to compute eddy covariance fluxes of NO_2. We presented the analysis of the NO_2 flux data along with eddy covariance fluxes of NO and O_3 in Horii et al. (2004); that analysis resulted in the net NO_x flux shown as part of the NO_y flux budget in this paper, which has taken into account the height difference between the inlets on the two separate towers.

A new capillary-column gas chromatograph with electron-capture detection (ECD), manufactured by Metcon Inc., was added to the Rohn tower in 2000. The ECD response and chromatographic separations were checked approximately monthly, or whenever operational settings were changed by calibration with PAN generated by photolysis of acetone in the presence of NO_2 (Warneck and Zerbach, 1992). The same NO standard used for NO_x and NO_y calibrations was delivered to the PAN calibrator and diluted to the desired concentration by mixing with zero air. A Hg-vapor lamp generated O_3 to convert NO to NO_2 and photolyzed acetone, which was supplied in excess of the NO. The yield of PAN was assumed to be close to 100%. The output of the PAN generator was delivered to the NO_x analyzer to confirm that there was no residual NO or NO_2 remaining. Each calibration run consisted of at least three concentrations that spanned the range of ambient values in order to verify a linear response. Detector response was determined from the slope of concentration versus signal.

2.3. Flux calculations

2.3.1. Eddy covariance fluxes of NO_y and NO_x

The computation of eddy covariance fluxes of NO_y and NO_x used vertical and horizontal wind velocities and virtual temperature measured by sonic anemometers at the same sampling heights as the trace gases (Rohn tower anemometer: Applied Technologies, SWS-211/3 K; scaffolding tower: Campbell Scientific, CSAT 3). Fluxes were calculated for 30-min periods from the covariance of linearly detrended time series for vertical velocity and trace gas concentration (Fan et al., 1990, 1992). To correct for instrument response functions derived from standard additions of the trace gases ($\sim$1 s exponential for NO_y and NO_x measured by chemiluminescence; $\sim$1 s exponential for NO_2 measured by the TDLAS), we applied a single-pole low-pass numerical filter to the virtual temperature time series, calculated the heat flux using the filtered data, and compared to the heat flux calculated using the unfiltered time series. The ratio of the two results provided an estimate of flux lost by instrumental smoothing of high-frequency fluctuations (Goulden et al., 1996; Munger et al., 1996). Corrections were typically less than 20% for both NO_x and NO_y. These calculations and corrections result in the eddy covariance fluxes reported here. Note that we do not report net ecosystem exchange, as no storage term is calculated, but that Munger et al. (1996) showed that storage at this site is small for NO_x and O_3.

2.4. Dry deposition inferential method for HNO_3

The hourly flux of HNO_3 was estimated from the measured concentration and a modeled deposition velocity obtained from a standard Dry Deposition Inferential Method approach, which treats the surface as a "big leaf" and addresses only the general properties of the lower atmosphere and surface, not their detailed structures. Developed in the context of SO_2 deposition by Wesely and Hicks (1977) and widely adopted thereafter for estimating fluxes of gases with little or no surface emission, versions of DDIM are currently used in routine monitoring networks such as CASTNet and in atmosphere–surface exchange models, either in the bulk form employed here or in multi-layer model applications (e.g. Wesely and Hicks, 2000; Baumgardner et al., 2002).

The DDIM treats the deposition velocity of a gas, V_d, in units of cm s^{-1}, as a set of three resistances in series, each of which depends on meteorological, site-specific, and/or species-specific conditions and parameters. The above-surface aerodynamic resistance, R_a, depends only on properties of the atmosphere. The diffusive boundary layer resistance, R_b, takes the molecular diffusivity of the particular gas into account. R_c represents a species-specific resistance to uptake by the particular surface elements present at the site. V_d is defined as a positive scalar representing a rate of transfer from the atmosphere to the surface:

$$V_d = (R_a + R_b + R_c)^{-1} \quad (1)$$

The product of a gas's deposition velocity and mixing ratio concentration, C, at a particular height provides an estimate of the mass flux density, F. By convention, we define downward fluxes (from atmosphere to surface) as negative:

$$F = -V_d C \quad (2)$$

where we report the flux in units of mol m^{-2} h^{-1}; we have applied a conversion using the molar volume of air at ambient temperature and pressure. R_a and R_b were calculated as follows, in units of s cm^{-1}, after Wesely and Hicks (1977), Hicks et al. (1987), Wesely (1989), and Meyers et al. (1989):

$$R_a = \frac{u}{(u^*)^2} - \frac{\psi_H}{ku^*} \quad (3)$$

$$\psi_H\,(\text{stable}) = \frac{-5(z-d)}{L} \quad (4a)$$

$$\psi_H\,(\text{unstable}) = \exp\left[0.598 + 0.39\ln\left(\frac{-(z-d)}{L}\right) - 0.09\left(\ln\left(\frac{-(z-d)}{L}\right)\right)^2\right] \quad (4b)$$

$$R_b \cong \frac{2}{ku^*}\left(\frac{Sc}{Pr}\right)^{2/3} \cong \frac{7.1}{u^*} \quad (5)$$

where u (cm s^{-1}) is the horizontal wind speed measured by the sonic anemometer; u^* (cm s^{-1}) the friction velocity ($u^* = (-1 \times \langle u'w' \rangle)^{1/2}$), where u' (cm s^{-1}) and w' (cm s^{-1}) are the deviations of horizontal and vertical wind speed, measured by sonic anemometry); k the von Karman's constant, 0.4; ψ_H a diabatic stability correction coefficient for heat transfer; z (m) the sensor height; d the zero-plane displacement height, approximately 19.8 m at Harvard Forest (Lefer, 1997); Sc the Schmidt number for HNO_3, 1.22; Pr the Prandtl number for air, 0.72; L (m) is the Monin–Obukhov length scale. Stable conditions are indicated by positive stability factor ζ (=z/L), unstable by negative ζ.

Due to the high solubility and surface reactivity of HNO_3, the approximation $R_c = 0$ is often made (Wesely and Hicks, 2000; Hanson and Lindberg, 1991). Meyers et al. (1989) found this assumption valid for a deciduous forest by comparing fluxes calculated from vertical concentration gradients with the modeled flux assuming $R_c = 0$; the observed deposition rate of HNO_3 was insensitive to LAI and controlled primarily by aerodynamic and diffusive processes rather than the particular characteristics of the surface. Although the approximation may not be valid for semi-arid coniferous forests due to accumulation of HNO_3 on foliage during dry periods (Tarnay et al., 2002), the available evidence suggests that it is suitable for the mixed deciduous and more humid environment at Harvard Forest.

Because we have made the approximation that R_c is negligible for HNO_3, the inferred deposition velocity depends sensitively on R_a and R_b. R_a in particular is known to be poorly approximated by (3) for very stable conditions and over uneven terrain (Brook et al., 1997; Wesely and Hicks, 2000). We observed such extreme stability only at night, with $u^* < 5$ cm s^{-1}, during fewer than 5% of nighttime hours during the sampling period. $V_d(HNO_3)$ may thus be underestimated in a small fraction of our data, but we do not expect the median results to be significantly affected. Although fluxes estimated using the DDIM may not capture the full range of short-term variability present in the natural atmosphere, they have been shown to be reasonably accurate in representing mean HNO_3 deposition to a forested surface (Pryor and Klemm, 2004).

3. Results and discussion

3.1. HNO_3 concentrations and inferred fluxes

Fig. 2 shows mean and median diel concentrations and inferred deposition velocities for HNO_3 by wind sector and season in 2000. We have plotted $-V_d$ so that negative values represent deposition in the figures. Fig. 3 displays the median diel cycles of all concentration data, inferred deposition velocities, and fluxes

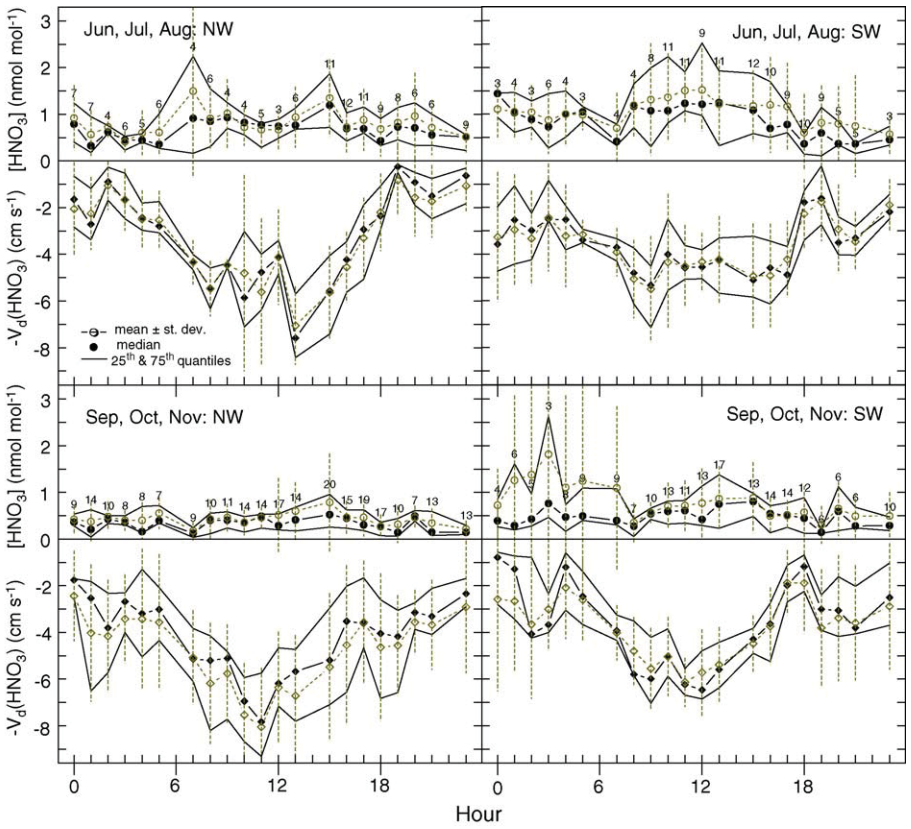

Fig. 2. Mean (open symbols, dashed lines) and median (solid symbols, solid lines) diel concentrations and inferred deposition velocities of HNO_3 separated by wind sector and season. Left panels: Northwest = 270–45°; right panels: Southwest = 180–270°; top panels: June–August; bottom panels: September–November. Solid traces above and below the medians represent 25th and 75th quantiles. Dashed vertical lines represent the standard deviations of the means. The number of hours of data for each hour of the day are shown above the HNO_3 concentrations.

calculated according to Eq. (2), segregated by wind sector only.

The diel cycle of HNO_3 concentration measured by the TDLAS was weak for both seasons and wind sectors. This finding is in contrast to Lefer and Talbot (1999), where a pronounced enhancement in daytime HNO_3 concentration was reported during the summer at Harvard Forest between 1991 and 1995, as measured by a mist chamber collection with analysis of NO_3^- by ion chromatography. We also found remarkably little difference in the observed HNO_3 concentration between Northwest and Southwest flow regimes, also in contrast to Lefer and Talbot (1999), where higher concentrations were reported for the Southwest sector. While the mist chamber technique has been employed and tested extensively in a variety of environments (e.g. Talbot et al., 1992, 1997; Lefer et al., 1994), its use of prefilters, longer sampling times, and detection of NO_3^- in solution create more opportunities for artifacts than the unfiltered inlet system and unique spectroscopic identification of the gas-phase HNO_3 molecule in the TDLAS instrument. As will be discussed in Section 3.2, the HNO_3 concentrations reported by the TDLAS are consistent within the context of the NO_y concentration and flux budgets and other recent observations of organic nitrates.

Unlike the HNO_3 concentration, the inferred HNO_3 deposition velocity had a strong diel cycle for both seasons and wind sectors, driven by larger daytime u^*. $V_d(HNO_3)$ varied between approximately 2 cm s^{-1} at night and 8 cm s^{-1} during the day. These inferred values are consistent with previous estimates using flux-gradient measurements, surrogate surfaces, and versions of the DDIM, in which $V_d(HNO_3)$ has been reported between 2 and 10 cm s^{-1} to forested landscapes, crops, and other surfaces (Hanson and Lindberg, 1991 and references therein; Sievering et al., 2001; Raymond et al., 2004; Pryor and Klemm, 2004).

The diel cycle in the HNO_3 flux inferred from Eqs. (1)–(5) (Fig. 3) is driven primarily by variations in atmospheric turbulence, as reflected in the deposition velocity. The sample time series in Fig. 4 shows that inferred HNO_3 flux and the eddy covariance NO_y flux

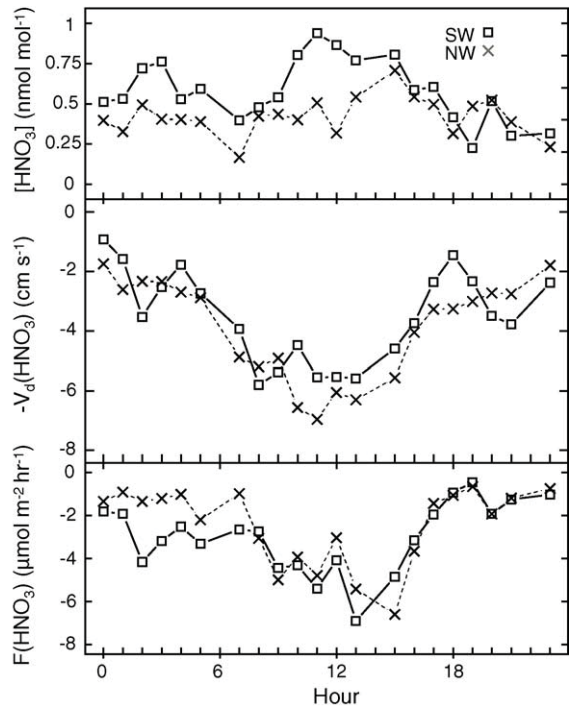

Fig. 3. Median diel HNO_3 concentration (upper panel), inferred deposition velocity (center panel), and flux (lower panel) for Southwest and Northwest wind sectors, June–November 2000.

follow one another closely, with only a few instances where the inferred HNO_3 flux exceeds the measured NO_y flux. Conditions when deposition of NO_y greatly exceeds the sum of measured, inferred, and estimated fluxes of NO_x and HNO_3 are discussed in Section 3.2.

The hourly time resolution of the Harvard Forest TDLAS HNO_3 dataset allows for testing of the DDIM for potential bias as it is currently employed in dry deposition measurement networks where filter packs are left in place for seven days at a time to measure average weekly concentrations (e.g. Clarke et al., 1997; Meyers et al., 1998). In the case of SO_2, the diel concentration and inferred deposition velocity have been shown to correlate strongly, with highest values in the daytime. Thus, when average weekly SO_2 concentration is used to calculate the flux, $F(SO_2)$ can be systematically underestimated by as much as 40% (Matt and Meyers, 1993). Sickles and Shadwisk (2002) tested the single weekly filter pack sampling method against the use of separate week-long daytime and nighttime filter packs and found evidence of bias in the resulting HNO_3 deposition results, likely due to chemical artifact formation on the filters. The Harvard Forest HNO_3 dataset eliminates the problem of chemical interference due to its definitive spectroscopic measurement of HNO_3.

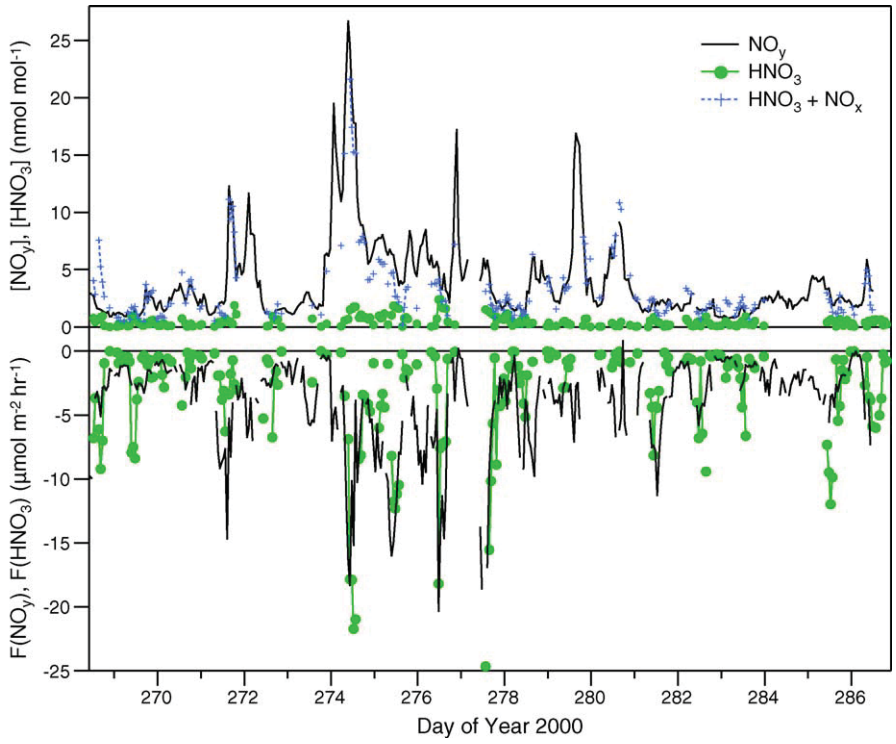

Fig. 4. Time series from 25 September to 12 October 2000. $[NO_y]$ and $[HNO_3]$ are in the upper panel, along with $[HNO_3] + [NO_x]$. Eddy covariance NO_y flux and inferred HNO_3 flux are shown in the lower panel.

We defined a "data week" for Harvard Forest beginning and ending on Tuesdays at 9:00 a.m. local time for June–November 2000, conforming to the standard employed by CASTNet. Data days begin and end at midnight Eastern Standard Time. For days with more than 5 h of HNO_3 concentration data, and weeks with more than 10 h of data (20 weeks), we calculated daily and weekly average (A) and integrated (I) fluxes using the hourly inferred deposition velocities and weekly average or hourly concentrations according to (6) and (7).

$$A = \frac{1}{N_{\text{hours}}} \sum_{\text{hour}} (-V_{\text{d(hour)}}) \overline{[\text{HNO}_3]_{\text{week}}} \quad (6)$$

$$I = \frac{1}{N_{\text{hours}}} \sum_{\text{hour}} (-V_{\text{d(hour)}}) [\text{HNO}_3]_{\text{hour}} \quad (7)$$

Although no days or weeks were completely free of data gaps, the distribution of gaps was random over all hours of the day and night, and the weekly correlation coefficient of deposition velocity with concentration neither increased nor decreased with the number of data hours used in the calculations.

Fig. 5 shows the fluxes inferred using daily and weekly averaged concentrations versus fluxes using hourly HNO_3 data and then summed to the same time intervals. Results fall near the 1:1 line for both daily and hourly aggregation times. The daily and weekly residuals ($A - I$) appear near-normally distributed,

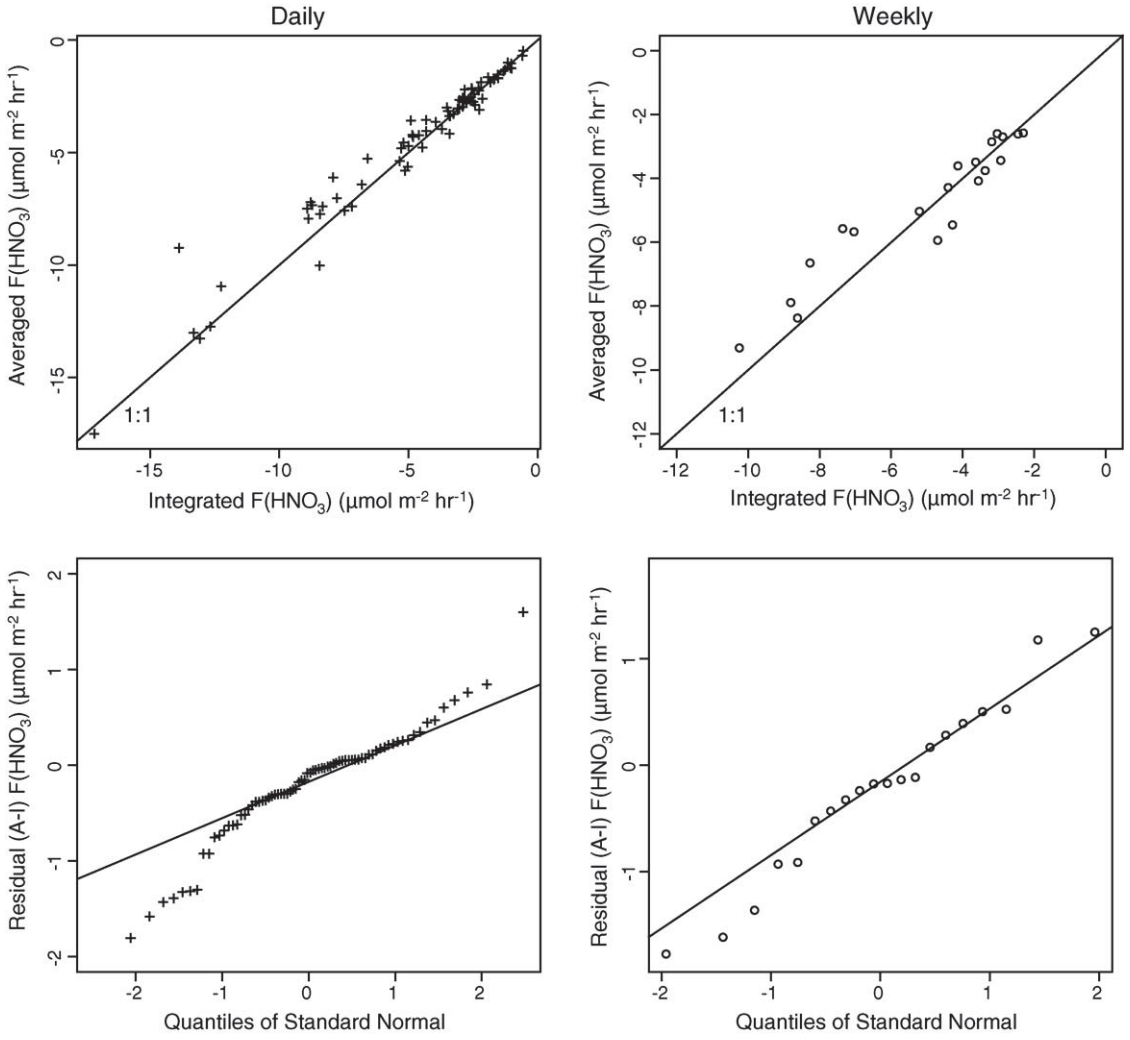

Fig. 5. Upper plots: daily (left) and weekly (right) averaged inferred fluxes vs. integrated inferred fluxes, with 1:1 line. Lower plots: daily (left) and weekly (right) residual integrated minus averaged HNO_3 flux vs. quantiles of the Standard Normal. Residuals appear near normally distributed.

with extended wings in the daily case. The mean (± 1 standard deviation) correlation coefficients of the deposition velocity and concentration on daily and weekly timescales, $r(V_d, HNO_3)_{daily} = -0.1 \pm 0.5$ and $r(V_d, HNO_3)_{weekly} = 0.1 \pm 0.3$, indicate no significant correlation on either timescale (see also Fig. 3). For weeks with 20 or more hours of data, $r(V_d, HNO_3)_{weekly}$ was as large as ± 0.5, but unlike results for SO_2 (Matt and Meyers, 1993), there was no consistently positive or negative correlation. Thus, it appears that differences between A and I were largely due to random errors in both deposition velocity and concentration.

These results support application of DDIM to estimate fluxes of HNO_3 from average concentration data as long as the concentration measurement method reports only gas-phase HNO_3 and the diel cycle is weak, as observed at Harvard Forest. Covariance between HNO_3 concentration and deposition velocity was notably weaker than for SO_2, and thus there was not a significant bias when computing weekly average flux using weekly average concentrations, compared to weekly integrated flux computed from hourly data. This result derives from the observation that nighttime concentrations of HNO_3 were not significantly smaller than daytime values at Harvard Forest, despite the strong adsorption of HNO_3 on surfaces and shallow nocturnal inversions. As noted by Munger et al. (1998), there is significant production of HNO_3 from the reaction of abundant NO_2 and O_3 at night at Harvard Forest, and it is likely that this production balances the small loss of HNO_3 by surface deposition, coincidentally improving the accuracy of the DDIM flux inferences.

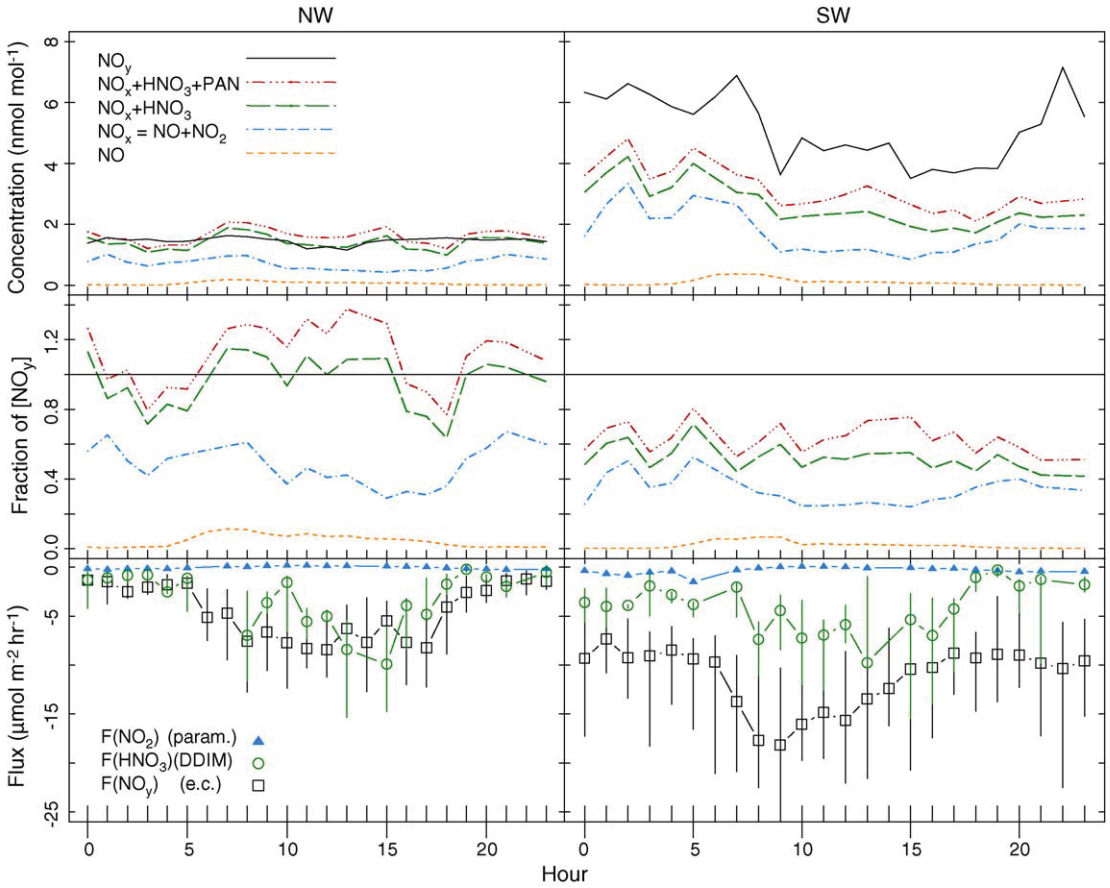

Fig. 6. Summer (June–August) 2000 median concentrations (upper panels), fractions of NO_y (middle panels), and fluxes (lower panels) of NO_y and component species separated by wind direction (Northwest on the left and Southwest on the right). Vertical lines in the flux panels show 25th and 75th quantiles of $F(NO_y)$ and $F(HNO_3)$; negative fluxes represent deposition; $F(NO_x)$ is derived from eddy covariance $F(NO)$ and $F(NO_2)$ measurements (corrected for photochemical cycling), $F(HNO_3)$ is inferred, and $F(NO_y)$ was measured by eddy covariance. The sum of NO_x, HNO_3, and PAN accounts for all of the NO_y concentration and flux for Northwesterly (unpolluted background) flows, whereas up to 50% of NO_y and $F(NO_y)$ under Southwesterly flows are in the form of reactive nitrogen species whose fluxes are not measured or estimated here.

3.2. NO_y concentration and flux budgets

Figs. 6 and 7 display median diel concentrations and fluxes of NO_y and all available individually measured or estimated constituents (NO, NO_2, HNO_3, and PAN) for Northwest and Southwest wind sectors during the summer (June–August) and fall (September–November) of 2000. The net NO_x flux is derived from eddy covariance measurements of NO, NO_2, and O_3, corrected for photochemical cycling between NO and NO_2 (Horii et al., 2004). Table 1 summarizes the fractional contributions of NO_x, HNO_3, and PAN to total NO_y concentration and flux by wind sector, day and night, and season, obtained by finding the slope m of the linear regressions to the hourly data, $C_i = m \cdot [NO_y]$ and $F_i = n \cdot F(NO_y)$.

During Northwesterly flow conditions, the sum of individual reactive nitrogen species, $\sum[NO_y]_i = [NO] + [NO_2] + [HNO_3] + [PAN]$, was very close to the observed concentration of NO_y. In this wind sector, HNO_3 accounted for roughly one-third of NO_y during the day in summer, one-fifth in the fall, with the remainder of the NO_y budget consisting largely of NO_x. The summertime concentration of PAN was on the order of 13% of NO_y. The Northwesterly NO_y flux was also dominated by HNO_3 deposition in both seasons.

During Southwesterly flow conditions, we found a significantly larger fraction of the NO_y concentration and flux in the form of unmeasured species. HNO_3 and NO_x contributed less than 70% of the total NO_y concentration, with summertime PAN accounting for 7–14%. The concentration of NO_y not accounted for in individual measurements was between 1 and 3 nmol mol^{-1} during the summer. Hayden et al. (2003) found a similar shortfall in their NO_y concentration budget at a site North of Harvard Forest in Quebec, with 25–30% of NO_y during the spring and summer not attributable to NO_x, HNO_3, and PAN. In another recent NO_y concentration speciation experiment at a forested site in Michigan, Thornberry et al. (2001) found a possible shortfall of approximately 20% between total NO_y and the sum of individually measured species NO_x, HNO_3, PAN, PPN, MPAN,

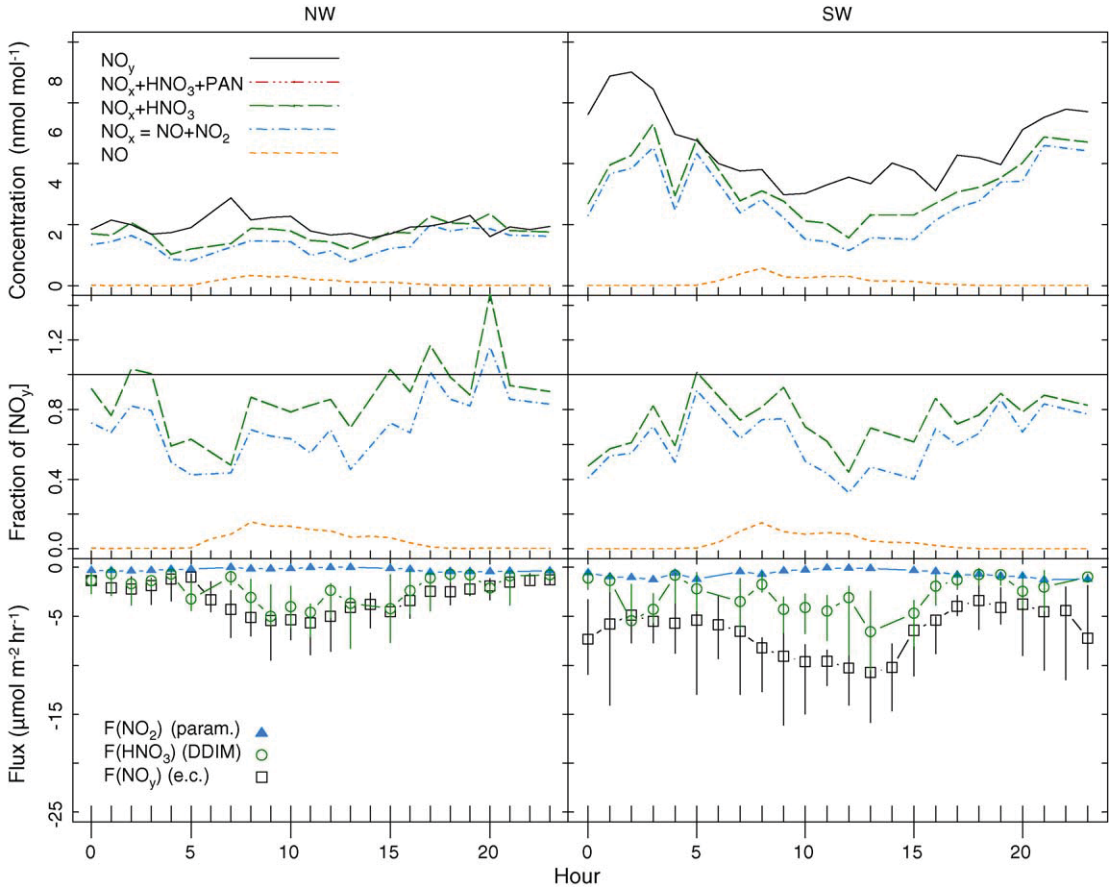

Fig. 7. Same format as Fig. 6 for fall (September–November) 2000. PAN concentrations were not measured during the fall of 2000.

Table 1
Fractional concentrations and fluxes of reactive nitrogen species at Harvard Forest, 2000

Slope ± standard error (*p*-value)	NW		SW	
	Day	Night	Day	Night
(a) Summer				
$[NO_x]/[NO_y]$	0.38 ± 0.02 (<1E−4)	0.56 ± 0.02 (<1E−4)	0.39 ± 0.02 (<1E−4)	0.46 ± 0.01 (<1E−4)
$[HNO_3]/[NO_y]$	0.35 ± 0.05 (<1E−4)	0.28 ± 0.04 (<1E−4)	0.20 ± 0.02 (<1E−4)	0.19 ± 0.02 (<1E−4)
[PAN]/$[NO_y]$	0.133 ± 0.008 (<1E−4)	0.131 ± 0.005 (<1E−4)	0.138 ± 0.009 (<1E−4)	0.069 ± 0.005 (<1E−4)
$([NO_x] + [HNO_3])/[NO_y]$	0.61 ± 0.09 (3E−4)	0.8 ± 0.2 (1E−3)	0.70 ± 0.05 (<1E−4)	0.69 ± 0.04 (<1E−4)
$F(NO_x)/F(NO_y)$	0.004 ± 0.002 (0.14)	0.042 ± 0.008 (<1E−4)	0.010 ± 0.003 (6E−4)	0.059 ± 0.004 (<1E−4)
$F(HNO_3)/F(NO_y)$	0.7 ± 0.1 (<1E−4)	0.2 ± 0.2 (0.4)	0.46 ± 0.06 (<1E−4)	0.6 ± 0.1 (<1E−4)
$(F(NO_x) + F(HNO_3))/F(NO_y)$	0.8 ± 0.1 (<1E−4)	0.2 ± 0.2 (0.3)	0.54 ± 0.06 (<1E−4)	0.5 ± 0.1 (1E−4)
(b) Fall				
$[NO_x]/[NO_y]$	0.83 ± 0.05 (<1E−4)	0.65 ± 0.04 (<1E−4)	0.73 ± 0.02 (<1E−4)	0.58 ± 0.03 (<1E−4)
$[HNO_3]/[NO_y]$	0.21 ± 0.03 (<1E−4)	0.14 ± 0.03 (<1E−4)	0.09 ± 0.01 (<1E−4)	0.11 ± 0.01 (<1E−4)
$([NO_x] + [HNO_3])/[NO_y]$	1.03 ± 0.07 (<1E−4)	0.97 ± 0.06 (<1E−4)	0.84 ± 0.02 (<1E−4)	0.70 ± 0.03 (<1E−4)
$F(NO_x)/F(NO_y)$	0.010 ± 0.007 (0.16)	0.21 ± 0.03 (<1E−4)	0.09 ± 0.02 (<1E−4)	0.11 ± 0.02 (<1E−4)
$F(HNO_3)/F(NO_y)$	0.7 ± 0.1 (<1E−4)	0.40 ± 0.09 (1E−4)	0.73 ± 0.07 (<1E−4)	0.38 ± 0.07 (<1E−4)
$(F(NO_x) + F(HNO_3))/F(NO_y)$	0.7 ± 0.1 (<1E−4)	0.6 ± 0.1 (<1E−4)	0.8 ± 0.1 (<1E−4)	0.59 ± 0.09 (<1E−4)

(a) Summer includes data from June to August. (b) Fall includes September–November. Linear regressions of the forms $C_i = m \cdot [NO]_y$ and $F_i = n \cdot F(NO_y)$ were computed on hourly data. PAN is not included in summations due to an insufficient number of overlapping data hours. Day: 08:00–16:00 h Eastern Standard Time. Night: 20:00–04:00 h EST.

C_3–C_5 alkyl nitrates, isoprene nitrates, HONO, and particulate NO_3^- and NO_2^-, but could not conclusively rule out interferences in one or more of the measurements.

At Harvard Forest, the NO_y discrepancy, $[NO_y] - \sum[NO_y]_i$, did not exhibit significant diel variation**,** but exhibited positive correlations with air temperature, H_2O vapor pressure, and O_3, which are all elevated during Southwesterly flows. HNO_3 flux was between 38 and 73% of $F(NO_y)$. Net $F(NO_x)$ was too small to account for the remaining NO_y deposition. Recent measurements of PAN deposition to vegetation imply deposition velocities between 0 and 1.5 cm s^{-1}, with strong control by leaf stomatal aperture and wide variability among species (Sparks et al., 2003). Although these results suggest that some of the unspeciated daytime NO_y flux at Harvard Forest may have been due to PAN uptake by vegetation, PAN cannot explain the continued nighttime deposition and appears too small to account for even the daytime flux discrepancy at our measured PAN concentrations. The inferred deposition velocity for unmeasured NO_y species was approximately 3 cm s^{-1}, similar to $V_d(HNO_3)$ (Figs. 2 and 3).

Because $F(HNO_3)/F(NO_y)$ was smaller for the warmer, moister Southwesterly conditions, while inferred $V_d(HNO_3)$ for the two wind sectors were nearly identical, we must consider the possibility of an inlet HNO_3 artifact related to varying temperature and humidity. Laboratory tests of the coated quartz TDLAS inlet at typical ambient temperature and humidity showed no significant permanent wall losses (Horii, 2002), but Neuman et al. (1999) noted a dramatic difference between the transmission of HNO_3 through Teflon fluoropolymer (PFA) tubing in dry versus humidified synthetic air. Moreover, the range of observed H_2O vapor pressures at Harvard Forest overlaps considerably between the wind sectors. During the measurement period (June–November 2000), the mean ± standard deviation H_2O vapor pressure for the Northwest sector was 1.5 ± 0.4 kPa, and 1.9 ± 0.4 kPa for the Southwest sector. In Fig. 8, summer (June–August) $F(HNO_3)/F(NO_y)$ is shown as a function of H_2O vapor pressure for both wind sectors. Although the fractional HNO_3 flux drops slightly at the highest H_2O vapor pressures observed under Northwesterly conditions, it is consistently lower under Southwesterly conditions across all H_2O vapor pressures. Hence, we cannot rule out small water vapor effects on HNO_3 transmission in the TDLAS, but the difference in $F(HNO_3)/F(NO_y)$ between the wind sectors cannot be attributed to such an effect.

Artifacts due to catalytic NO_y converters have been implicated in some studies where the sum of individual reactive nitrogen species was substantially less than the observed concentration of NO_y. However, it is unlikely that this is the cause of the discrepancy observed in the Southwest sector at Harvard Forest. Kliner et al. (1997)

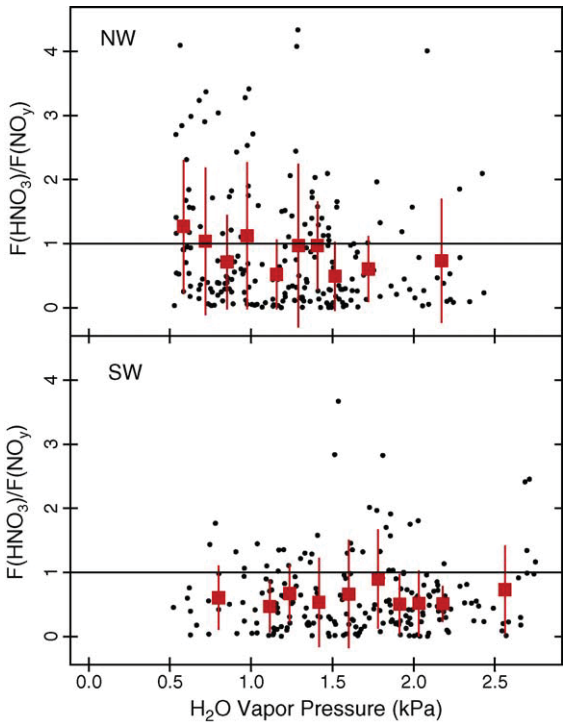

Fig. 8. Fraction of HNO_3 flux (inferred) to NO_y flux (eddy covariance) as a function of H_2O vapor pressure for the Northwest (upper) and Southwest (lower) wind sectors at Harvard Forest, summer 2000. Dots represent individual hourly values, and squares with vertical bars represent means and standard deviations of the fractional flux binned by quantiles of H_2O vapor pressure.

found that conversion of reduced nitrogen species HCN, CH_3CN, and NH_3 (not included as NO_y) on a hot 24 karat Au catalyst in the presence of H_2, as used at Harvard Forest, was exacerbated after cleaning the catalyst and by very low humidity. The catalyst at Harvard Forest is well-aged, and as noted above, ambient conditions are never very dry. In addition, NH_3 concentrations during the summer at Harvard Forest are significantly less than 1 nmol mol^{-1} ($[NH_3] \approx 0.2$–0.4 nmol mol^{-1}, independent of wind direction; see Lefer and Talbot, 1999), far too small to influence these results even if some NH_3 were oxidized to NO in the catalyst.

Particulate NO_3^- also contributes to the total NO_y measurement, but was not independently monitored at our site in 2000. Lefer and Talbot (2001) measured aerosol nitrate periodically during the summers of 1991–1995 and report a median value ~5 nmol m^{-3} (0.1 nmol mol^{-1}) for the Northwest wind sector, and ~10 nmol m^{-3} (0.2 nmol mol^{-1}) for the Southwest. These concentrations of particulate NO_3^- appear much too low to account for the observed discrepancy between species sums and total NO_y for the Southwest sector.

Munger et al. (1996) defined the deposition velocity $V_d(NO_y–NO_x)$ for NO_y species excluding NO_x as $F(NO_y)/([NO_y] - [NO_x])$. They found that $V_d(NO_y–NO_x)$ varied little between Northwest and Southwest wind sectors at Harvard Forest, in harmony with the inferred deposition velocities of HNO_3 and non-HNO_3 depositing species analyzed here. Chemical species combining products of organic hydrocarbon oxidation with NO_2, such as alkyl and hydroxyalkyl nitrates, are likely to be efficient surface depositors, particularly the hydroxyalkyl nitrates due to their high solubility and low vapor pressure (Shepson et al., 1996; Treves et al., 2000). Munger et al. (1998) estimated production rates of hydroxyalkyl nitrates from biogenic emissions of isoprene and monoterpenes at Harvard Forest, and found that they could account for approximately 25% of the observed NO_y deposition during the summer, consistent with other recent observations of alkyl nitrates at rural field sites (Grossenbacher et al., 2001; Day et al., 2003; Rosen et al., 2004). The flux budgets presented here, including the inferred HNO_3 fluxes, provide strong support for the role of hydroxy alkyl nitrates to deposition processes for Southwesterly (polluted) flows at Harvard Forest.

4. Conclusions

We found that HNO_3 concentrations and fluxes were independent of wind direction and showed little difference between the clean and polluted wind sectors at Harvard Forest. The higher NO_y deposition rates associated with Southwesterly flow arose primarily from rapidly depositing, non-HNO_3 species. The concentrations of unmeasured species in our observations are consistent with recent data for the sum of alkyl- and hydroxyalkyl nitrites at urban and rural locations reported by Day et al. (2003) and our flux data suggest that these compounds deposit to the forest with similar velocities as HNO_3 (~3 cm s^{-1}). Their presence in the Southwesterly flow regime suggests that the higher temperatures and NO_x concentrations present in this air may enhance formation of organic nitrates during the oxidation of forested-derived biogenic hydrocarbons such as isoprene and monoterpenes. Anthropogenic hydrocarbons may also contribute.

It is not known whether the non-HNO_3 depositors whose presence we have inferred would produce a signal in filter pack, denuder, or mist chamber HNO_3 measurements. Although dissolution to form NO_3^- in

solution is possible, we do not know if the efficiency for this process could be comparable to HNO_3. The unidentified species could potentially produce significant artifacts in the measurements of total dry deposition of reactive nitrogen using filter pack HNO_3 + particulate $(NO_3^- + NH_4^+)$ measurements (e.g. Pratt et al., 1996). For conditions with large biogenic hydrocarbon sources and moderate transport of anthropogenic NO_x, estimates of dry nitrogen deposition might be significantly in error if they do not include species like the hydroxyalkyl nitrates.

HNO_3 concentration measurements above the canopy at Harvard Forest imply that the conventional Dry Deposition Inferential Method used to estimate the deposition flux of HNO_3 would have been reliable during the summer and fall of 2000, provided that the time-averaged measurements were specific for HNO_3. The diurnal variation of HNO_3 concentration was weak, and thus the DDIM applied in a weekly average sense to our hourly data, analogous to the practice at nitrogen deposition network sites, introduced random errors but not a persistent bias. Since the weak diurnal variation of HNO_3 concentration may reflect nocturnal production, the general application of this result requires measurements at other sites, e.g. by day/night sampling. If filter packs had unit efficiency for measuring non-HNO_3 compounds, they might coincidentally give values for deposition flux close to NO_y deposition, but the flux would not be attributable to HNO_3 or any other specific compound.

Acknowledgements

This work was supported by NASA Headquarters under the Earth System Science Fellowship Grant NGT5-30205, by the NOAA Global Change Program Grant NA46GP0119, by the National Science Foundation Grant ATM-9981282, and by the Office of Science, Biological and Environmental Research Program (BER), U.S. Department of Energy, through the Northeast Regional Center of the National Institute for Global Environmental Change (NIGEC) under the Cooperative Agreement No. DE-FC02-03ER6313. The authors gratefully acknowledge the assistance of Aerodyne Research staff members Jeff Mulholland and Bob Prescott, and Harvard University engineers Alfram Bright and Bruce Daube, for their work on the TDLAS instrument, and thank John Budney, Elaine Gottleib, Jack Edwards, Edythe Ellin, Don Hesselton, Felicia Frizzell, and Shane Heath for their support at the HFEMS.

References

Aber, J., McDowell, W., Nadelhoffer, K., Magill, A., Bernston, G., Kamekea, M., McNulty, S., Currie, W., Rustad, L., Fernandez, I., 1998. Nitrogen saturation in temperate forest ecosystems—hypotheses revisited. Bioscience 48, 921–934.

Aneja, V.P., Kim, D.-S., Das, M., Hartsell, B.E., 1996. Measurements and analysis of reactive nitrogen species in the rural troposphere of southeast United States: Southern Oxidant Study Site SONIA. Atmos. Environ. 30, 649–659.

Baumgardner, R.E., Lavery, T.F., Rogers, C.M., Isil, S.S., 2002. Estimates of the atmospheric deposition of sulfur and nitrogen species: Clean Air Status And Trends Network, 1990–2000. Environ. Sci. Technol. 36, 2614–2629.

Bradshaw, J., Sandholm, S., Talbot, R., 1998. An update on reactive odd-nitrogen measurements made during recent NASA Global Tropospheric Experiment programs. J. Geophys. Res. 103, 19129–19148.

Bradshaw, J., Davis, D., Grodzinsky, G., Smyth, S., Newell, R., Sandholm, S., Liu, S., 2000. Observed distributions of nitrogen oxides in the remote free troposphere from the NASA Global Tropospheric Experiment Programs. Rev. Geophys. 38, 61–116.

Brook, J.R., Di-Giovanni, F., Cakmak, S., Meyers, T.P., 1997. Estimation of dry deposition velocity using inferential models and site-specific meteorology—uncertainty due to siting of meteorological towers. Atmos. Environ. 31, 3911–3919.

Clarke, J.F., Edgerton, E.S., Martin, B.E., 1997. Dry deposition calculations for the Clean Air Status And Trends Network. Atmos. Environ. 31, 3667–3678.

Day, D.A., Dillon, M.B., Wooldridge, J., Thornton, J.A., Rosen, R.S., Wood, E.C., Cohen, R.C., 2003. On alkyl nitrates, O3, and the "missing NOy". J. Geophys. Res. 108 (D16). doi:10.1029/2003JD003685, 4501.

Fan, S.-M., Wofsy, S.C., Bakwin, P.S., Jacob, D.J., Fitzjarrald, D.R., 1990. Atmosphere–biosphere exchange of CO_2 and O_3 in the central Amazon forest. J. Geophys. Res. 95, 16851–16864.

Fan, S.-M., Wofsy, S.C., Bakwin, P.S., Jacob, D.J., Anderson, S.M., Kebabian, P.L., McManus, J.B., Kolb, C.E., Fitzjarrald, D.R., 1992. Micrometeorological measurements of CH_4 and CO_2 exchange between the atmosphere and the subarctic tundra. J. Geophys. Res. 97, 16627–16643.

Fehsenfeld, F.C., Huey, L.G., Sueper, D.T., Norton, R.B., Williams, E.J., 1998. Ground-based intercomparison of nitric acid measurement techniques. J. Geophys. Res. 103, 3343–3353.

Furutani, H., Akimoto, H., 2002. Development and characterization of a fast measurement system for gas-phase nitric acid with a chemical ionization mass spectrometer in the marine boundary layer. J. Geophys. Res. 107 (D2). doi:10.1029/2000JD000269, 4016.

Goulden, M.L., Munber, J.W., Fan, S.-M., Daube, B.C., Wofsy, S.C., 1996. Measurements of carbon storage by long-term eddy correlation: methods and a critical evaluation of accuracy. Global Change Biol. 2, 169–182.

Grossenbacher, J.W., Shepson, P.B., Thornberry, T., Witmer-Rich, M., Carroll, M.A., Faloona, I., Tan, D., Brune, W., Apel, E., Riemer, D., Westberg, H.A., 2001. Measurements of isoprene nitrates above a forest canopy. J. Geophys. Res. 106, 24429–24438.

Harrison, R.M., Grenfell, J.L., Yamulki, S., Clemitshaw, K.C., Penkett, S.A., Cape, J.N., McFadyen, G.G., 1999. Budget of NO_y species measured at a coastal site. Atmos. Environ. 33, 4255–4272.

Hanson, P., Lindberg, S.E., 1991. Dry deposition of reactive nitrogen compounds: a review of leaf, canopy, and non-foliar measurements. Atmos. Environ. 25A, 1615–1634.

Hayden, K.L., Anlauf, K.G., Hastie, D.R., Bottenheim, J.W., 2003. Partitioning of reactive atmospheric nitrogen oxides at an elevated site in southern Quebec, Canada. J. Geophys. Res. 108 (D19). doi:10.1029/2002JD003188, 4603.

Hicks, B.B., Baldocchi, D.D., Meyers, T.P., Hosker Jr., R.P., Matt, D.R., 1987. A preliminary multiple resistance routine for deriving dry deposition velocities from measured quantities. Water Air Soil Pollut. 36, 311–330.

Horii, C.V., Zahniser, M., Nelson, D., McManus, J.B., Wofsy, S.C., 1999. Nitric acid and nitrogen dioxide flux measurements: a new application of Tunable Diode Laser Absorption Spectroscopy. Proc. SPIE 3758, 152–161.

Horii, C.V., 2002. Tropospheric reactive nitrogen speciation, deposition, and chemistry at Harvard Forest. Ph.D. Thesis. Harvard University, Cambridge, MA.

Horii, C.V., Munger, J.W., Wofsy, S.C., Zahniser, M., Nelson, D., McManus, J.B., 2004. Fluxes of nitrogen oxides over a temperate deciduous forest. J. Geophys. Res. 109 (D8). doi:10.1029/2003JD004326, D08305.

Huey, L.G., Dunlea, E.J., Lovejoy, E.R., Hanson, D.R., Norton, R.B., Fehsenfeld, F.C., Howard, C.J., 1998. Fast time response measurements of HNO_3 in air with a chemical ionization mass spectrometer. J. Geophys. Res. 103, 3355–3360.

Kliner, D.A.V., Daube, B.C., Burley, J.D., Wofsy, S.C., 1997. Laboratory investigation of the catalytic reduction technique for measurement of atmospheric NO_y. J. Geophys. Res. 102, 10759–10776.

Lefer, B.L., Talbot, R.W., Harriss, R.C., Bradshaw, J.D., Sandholm, S.T., Olson, J.O., Sachse, G.W., Collins, J., Shipham, M.A., Blake, D.R., Klemm, K.I., Klemm, O., Gorzelska, K., Barrick, J., 1994. Enhancement of acidic gases in biomass-burning impacted air masses over Canada. J. Geophys. Res. 99, 1721–1738.

Lefer, B.L., December 1997. The chemistry and dry deposition of atmospheric nitrogen at a rural site in the northeastern United States. Ph.D. Thesis. University of N.H., Durham, 119 pp.

Lefer, B.L., Talbot, R.W., 1999. Nitric acid and ammonia at a rural northeastern U.S. site. J. Geophys. Res. 104, 1645–1661.

Lefer, B.L., Talbot, R.W., 2001. Summertime measurements of aerosol nitrate and ammonium at a northeastern U.S. site. J. Geophys. Res. 106, 20365–20378.

Magill, A.H., Aber, J.D., Bernston, G.M., McDowell, W.H., Nadelhofer, K.J., Melillo, J.M., Steudler, P., 2000. Long-term nitrogen additions and nitrogen saturation in two temperate forests. Ecosystems 3, 238–253.

Matt, D.R., Meyers, T.P., 1993. On the use of the inferential technique to estimate dry deposition of SO_2. Atmos. Environ. 27A, 493–501.

Mauldin III, R.L., Tanner, D.J., Eisele, F.L., 1998. A new chemical ionization mass spectrometer technique for the fast measurement of gas phase nitric acid in the atmosphere. J. Geophys. Res. 103, 3361–3367.

McFadyen, G.G., Neil Cape, J., 1999. Physical and chemical influences on PAN concentrations at a rural site. Atmos. Environ. 33, 2929–2940.

McManus, J.B., Kebabian, P.L., Zahniser, M.S., 1995. Astigmatic mirror multiple pass absorption cells for long pathlength spectroscopy. Appl. Opt. 34, 3336.

Meyers, T.P., Huebert, B.J., Hicks, B.B., 1989. HNO_3 deposition to a deciduous forest. Boundary-Layer Meteorol. 49, 395–410.

Meyers, T.P., Kinkelstein, P., Clarke, J., Ellestad, T.G., Sims, P.F., 1998. A multilayer model for inferring dry deposition using standard meteorological measurements. J. Geophys. Res. 103, 22645–22661.

Miller, T.M., Ballenthin, J.O., Meads, R.F., Hunton, D.E., Thorn, W.F., Viggiano, A.A., Kondo, Y., Koiki, M., Zhao, Y., 2000. Chemical ionization mass spectrometer technique for the measurement of HNO_3 in air traffic corridors in the upper troposphere during the SONEX campaign. J. Geophys. Res. 105, 3701–3707.

Moody, J.L., Munger, J.W., Goldstein, A.H., Jacob, D.J., Wofsy, S.C., 1998. Harvard Forest regional-scale air mass composition by Patterns in Atmospheric Transport History (PATH). J. Geophys. Res. 103, 13181–13194.

Moore, K.E., Fitzjarrald, D.R., Sakai, R.K., Goulden, M.L., Munger, J.W., Wofsy, S.C., 1996. Seasonal variation in radiative and turbulent exchange at a deciduous forest in central Massachusetts. J. Appl. Meteorol. 35, 122–134.

Munger, J.W., Wofsy, S.C., Bakwin, P.S., Fan, S.-M., Goulden, M.L., Daube, B.C., Goldstein, A.H., 1996. Atmospheric deposition of reactive nitrogen oxides and ozone in a temperate deciduous forest and a subarctic woodland: 1. Measurements and mechanisms. J. Geophys. Res. 101, 12639–12657.

Munger, J.W., Fan, S.-M., Bakwin, P.S., Goulden, M.L., Goltstein, A.H., Colman, A.S., Wofsy, S.C., 1998. Regional budgets for nitrogen oxides from continental sources: variations of rates for oxidation and deposition with season and distance from source regions. J. Geophys. Res. 103, 8355–8368.

Neuman, J.A., Huey, L.G., Ryerson, T.B., Fahey, D.W., 1999. Study of inlet materials for sampling atmospheric nitric acid. Environ. Sci. Technol. 33, 1133–1136.

Parrish, D.D., Buhr, M.P., Trainer, M., Norton, R.B., Shimshock, J.P., Fehsenfeld, F.C., Anlauf, K.G., Bottenheim, J.W., Tang, Y.Z., Wiebe, H.A., Roberts, J.M., Tanner, R.L., Newman, L., Bowersox, V.C., Olszyna, K.J., Bailey, E.M., Rodgers, M.O., Wang, T., Berresheim, H., Roychowdhury, U.K., Demerjian, K.L., 1993. The total reactive oxidized nitrogen levels and the partitioning between the individual species at six rural sites in eastern North America. J. Geophys. Res. 98, 2927–2939.

Pratt, G.C., Orr, E.J., Bock, D.C., Strassman, R.L., Fundine, D.W., Twaroski, C.J., Thornton, J.D., Meyers, T.P., 1996. Estimation of dry deposition of inorganics using filter pack data and inferred deposition velocity. Environ. Sci. Technol. 30, 2168–2177.

Pryor, S.C., Klemm, O., 2004. Experimentally derived estimates of nitric acid dry deposition velocity and viscous sub-layer resistance at a conifer forest. Atmos. Environ. 38, 2769–2777.

Raymond, H.A., Yi, S.-M., Moumen, N., Han, Y., Holsen, T.M., 2004. Quantifying the dry deposition of reactive nitrogen and sulfur containing species in remote areas using a surrogate surface analysis approach. Atmos. Environ. 38, 2687–2697.

Rosen, R.S., Wood, E.C., Wooldridge, P.J., Thornton, J.A., Day, D.A., Kuster, W., Williams, E.J., Jobson, B.T., Cohen, R.C., 2004. Observations of total alkyl nitrates during Texas Air Quality Study 2000: implications for O3 and alkyl nitrate photochemistry. J. Geophys. Res. 109 (D7). doi:10.1029/2003JD004227, D07303.

Rosman, K., Shimmo, M., Karlsson, A., Hansson, H.-C., Keronen, P., Allen, A., Hoenninger, G., 2001. Laboratory and field investigations of a new and simple design for the parallel plate denuder. Atmos. Environ. 35, 5301–5310.

Schrimpf, W., Lienaerts, K., Müller, K.P., Rudolph, J., Neubert, R., Schüßler, W., Levin, I., 1996. Dry deposition of peroxyacetyl nitrate (PAN): determination of its deposition velocity at night from measurements of the atmospheric PAN and ^{222}Radon concentration gradient. Geophys. Res. Lett. 23, 3599–3602.

Shepson, P.B., Bottenheim, J.W., Hastie, D.R., Venkatram, A., 1992. Determination of the relative ozone and PAN deposition velocities at night. Geophys. Res. Lett. 19, 1121–1124.

Shepson, P.B., Mackay, E., Muthuramu, K., 1996. Henry's Law constants and removal processes for several atmospheric β-hydroxy alkyl nitrates. Environ. Sci. Technol. 30, 3618–3623.

Sickles II, J.E., Shadwisk, D.S., 2002. Biases in Clean Air Status and Trends Network filter pack results associated with sampling protocol. Atmos. Environ. 36, 4687–4698.

Sievering, H., Kelly, T., McConville, G., Seibold, C., Turnipseed, A., 2001. Nitric acid dry deposition to conifer forests: Niwot Ridge spruce–fir–pine study. Atmos. Environ. 35, 3851–3859.

Sparks, J.P., Roberts, J.M., Monson, R.K., 2003. The uptake of gaseous organic nitrogen by leaves: a significant global nitrogen transfer process. Geophys. Res. Lett. 30 , doi:10.1029/2003GL018578.

Talbot, R.W., Vijgen, A.S., Harriss, R.C., 1992. Soluble species in the Arctic summer troposphere: acidic gases, aerosols, and precipitation. J. Geophys. Res. 97, 16531–16545.

Talbot, R.W., Dibb, J.E., Lefer, B.L., Scheuer, E.M., Bradshaw, J.D., Sandholm, S.T., Smyth, S., Blake, D.R., Blake, N.J., Sachse, G.W., Collins, J.E., Gregory, G.L., 1997. Large-scale distributions of tropospheric nitric, formic, and acetic acids over the western pacific basin during wintertime. J. Geophys. Res. 102, 28303–28313.

Tarnay, L.W., Gertler, A., Taylor Jr., G.E., 2002. The use of inferential models for estimating nitric acid vapor deposition to semi-arid coniferous forests. Atmos. Environ. 36, 3277–3287.

Thornberry, T., Carroll, M.A., Keeler, G.J., Sillman, S., Bertman, S.B., Pippin, M.R., Ostling, K., Grossenbacher, J.W., Shepson, P.B., Cooper, O.R., Moody, J.L., Stockwell, W.R., 2001. Observations of reactive oxidized nitrogen and speciation of NO_y during the PROPHET summer 1998 intensive. J. Geophys. Res. 106, 24359–24386.

Tomlinson, G.H., 2003. Acidic deposition, nutrient leaching and forest growth. Biogeochemistry 65, 51–81.

Treves, K., Shragina, L., Rudich, Y., 2000. Henry's Law constants of some β-, γ-, and δ-hydroxy alkyl nitrates of atmospheric interest. Environ. Sci. Technol. 34, 1197–1203.

U.S. Environmental Protection Agency, 2001. Atmospheric deposition of sulfur and nitrogen compounds. In: National Air Quality and Emission Trends Report, 1999, EPS454/R-01-004. Office of Air Quality Planning and Standards, Research Triangle Park, NC.

Warneck, P., Zerbach, T., 1992. Synthesis of peroxyacetyl nitrate in air by acetone photolysis. Environ. Sci. Technol. 26, 74–79.

Wesely, M.L., 1989. Parameterization of surface resistances to gaseous dry deposition in regional-scale numerical models. Atmos. Environ. 23, 1293–1304.

Wesely, M.L., Hicks, B.B., 1977. Some factors that affect the deposition rates of sulfur dioxide and similar gases on vegetation. J. Air Pollut. Control Assoc. 27, 1110–1116.

Wesely, M.L., Hicks, B.B., 2000. A review of the current status of knowledge on dry deposition. Atmos. Environ. 34, 2261–2282.